ROYAL SOCIETY
OF CHEMISTRY

Check for updates

Detachment of bovine corneal endothelial cell sheets by cooling-induced surface hydration of poly[(R)-3-hydroxybutyrate]-based thermoresponsive copolymer coating†

Wilson Wee Mia Soh, [a] Jingling Zhu, [ab] Xia Song, [a] Deepak Jain, [c] Evelyn K. F. Yim *[cde] and Jun Li *[ab]

Cell sheet technology (CST) is a fascinating scaffoldless tissue engineering technique to generate a physiologically representative tissue replacement from autologous sources. As compared to conventional enzymatic cell harvesting methods, CST enables the preservation of important cell-to-cell junctions and extracellular matrix (ECM) components. However, covalent grafting methods are often employed for CST. In this study, a series of triblock copolymers with a hydrophobic and biocompatible poly[(R)-3-hydroxybutyrate] (PHB) central block flanked by varying lengths of terminal poly(N-isopropylacrylamide) (PNIPAAm) blocks (PNIPAAm-PHB-PNIPAAm) was synthesized *via* atom transfer radical polymerization of NIPAAm. The thermoresponsive triblock copolymers were explored as a non-covalent surface coating for culturing and detaching bovine corneal endothelial cell (BCEC) sheets. Aqueous solutions of the triblock copolymers produced thermosensitive micelles which can be drop-casted on glass substrates, resulting in a temperature-responsive surface. Importantly, incorporating a central hydrophobic PHB block enabled the anchoring of the coating to the bare substrate and enhanced the proliferation rate of the BCECs studied. Effective detachment of an intact cell sheet was also demonstrated *via* a cooling treatment at 4 °C for 20 min, and the viability of the detached cell sheet was found to be unaffected by the cooling. This work may potentially inspire more studies involving the non-covalent thermoresponsive polymer coatings for corneal tissue engineering applications.

1. Introduction

Smart polymers are polymeric materials that reciprocate extrinsic stimuli (*e.g.*, temperature, light, magnetic field, and pH) with reversible changes in their physical and/or chemical characteristics.[1] Among them, temperature-responsive polymers have continued to receive wide interest and gain influential pertinence in numerous applications.[2–4] Importantly, polymers that are responsive to temperatures around 37 °C

such as poly(N-isopropylacrylamide) (PNIPAAm),[5] poly[oligo-(ethylene glycol) methacrylate] (POEGMA),[6] and poly(N-vinyl caprolactam) (PVCL)[7,8] have been extensively explored in the design of multifunctional smart materials for biomedical applications. Examples of such materials include injectable hydrogels,[9–13] microgels,[14] micellar drug delivery systems,[15–18] coatings,[19] surfaces,[20,21] and fluorescent polymeric thermometers.[22] Moreover, the temperature-responsive polymers can be copolymerized with distinct polymeric blocks to modulate and achieve tailored properties. For instance, PNIPAAm-PEG copolymer-based hydrogels exhibit a higher swelling ratio and stress dissipation properties as compared to their pristine homopolymer counterpart.[23] On the other hand, the introduction of hydrophobic and biodegradable polyesters such as poly(lactic acid) (PLA) and poly(ε-caprolactone) (PCL) can enhance thermosensitivity at a lower temperature range[24] and may permit safe *in vivo* biodegradation.[25]

One prominent application of temperature-sensitive polymers is the fabrication of smart surfaces for cell sheet technology (CST).[26,27] The CST is based on the property of the polymer, PNIPAAm, with reversible hydration states in response to

a Department of Biomedical Engineering, National University of Singapore, 15 Kent Ridge Crescent, Singapore 119276, Singapore. E-mail: jun-li@nus.edu.sg

b NUS Environmental Research Institute (NERI), National University of Singapore, 5A Engineering Drive 1, Singapore 117411, Singapore

c Department of Chemical Engineering, University of Waterloo, 200 University Avenue West, Waterloo, ON, N2L 3G1, Canada. E-mail: eyim@uwaterloo.ca

d Waterloo Institute for Nanotechnology, University of Waterloo, 200 University Avenue West, Waterloo, ON, N2L 3G1, Canada

e Center for Biotechnology and Bioengineering, University of Waterloo, 200 University Avenue West, Waterloo, ON, N2L 3G1, Canada

† Electronic supplementary information (ESI) available: Gel permeation chromatographs, TGA heating curves, ^{1}H NMR probe of micellar configuration, and ATR-FTIR characterization of substrates. See DOI: https://doi.org/10.1039/d2tb01926d

This journal is © The Royal Society of Chemistry 2022

J. Mater. Chem. B, 2022, **10**, 8407–8418 | 8407

temperature changes. PNIPAAm is a non-cytotoxic polymer that is water-soluble below its lower critical solution temperature (LCST) and exhibits phase separation in water above its LCST, forming large aggregates. By applying this unique property to cell culture substrates, a smart temperature-responsive surface can be generated. Above its LCST, PNIPAAm is hydrophobic and is conducive to extracellular matrix (ECM) adsorption to facilitate cell adhesion. When cooled below its LCST, PNIPAAm becomes hydrophilic and non-cell adhesive, detaching cells in the form of an interconnected cell sheet. This technology has garnered interest from researchers and biomedical manufacturers as the cell sheet is more physiologically representative as compared to single cells.[28–31] Additionally, typical methods of *in vitro* cell harvest involve enzymes like trypsin and dispase. However, enzymatic treatment results in a loss of important cell-to-cell junctions and ECM components which may be detrimental to the proper functioning of primary and stem cells.[32]

The corneal endothelium is a single layer of cells demarcating the interface between the cornea and the anterior chamber. The corneal endothelium's main role is to pump out excess fluid in the stroma to support optimal water content.[33] The maintenance of the stroma hydration state is essential to maintaining corneal optical clarity. The ATP pumps and tight junction proteins are thus imperative in ensuring the ideal performance of the corneal endothelium.[34] A major challenge of using human corneal endothelial cells as therapeutics is that they do not proliferate *in vivo*.[35] When cell loss occurs because of injury or disease, the endothelial cells compensate by cell migration and expansion instead of proliferating to fill up the gaps. Therefore, when significant cell loss happens, the barrier integrity of the corneal endothelium may be compromised, resulting in impairment of its pump function, causing stromal edema and

potentially vision loss. To this end, an implantable corneal endothelial cell sheet with preserved tight junctions and ECM is an attractive corneal endothelial tissue engineering solution. Currently, covalent grafting of PNIPAAm to cell culture substrates has been used as a strategy to create temperature-responsive surfaces for corneal endothelial tissue engineering.[36,37] However, covalent grafting often involves intricate procedures and techniques with irreversible processes. On the other hand, non-covalent surface coatings provide more flexibility in creating smart surfaces with the advantages such as the ease of adjusting coating densities and production scaling-up.

In our earlier studies, we successfully applied non-covalent surface coating of a PNIPAAm block copolymer functionalized by the hydrophobic and biocompatible poly[(R)-3-hydroxybutyrate] (PHB) to culture human mesenchymal and mouse embryonic stem cells and achieve enzyme-free cell detachment.[38,39] In this work, we propose to investigate the potential of the non-covalent polymer coating strategy for detaching bovine corneal endothelial cell sheets. To this end, we synthesized a series of triblock copolymers with PHB central block flanked by varying lengths of terminal PNIPAAm blocks (PNIPAAm-PHB-PNIPAAm) *via* atom transfer radical polymerization of NIPAAm using bromide-functionalized PHB and evaluated the copolymers as surface coatings for bovine corneal endothelial cell sheet application (Fig. 1). By utilizing the straightforward method of drop-casting to coat cell culture substrates, the production of the bovine corneal endothelial cell (BCEC) sheets will be much simpler and easier compared to the covalent grafting method. Notably, the hydrophobic PHB core acts as an anchor that secures the triblock copolymer to cell culture substrates *via* hydrophobic interactions. The corneal endothelial cells are then cultured to confluence on the temperature-responsive substrate, facilitated by the cell-adhesive
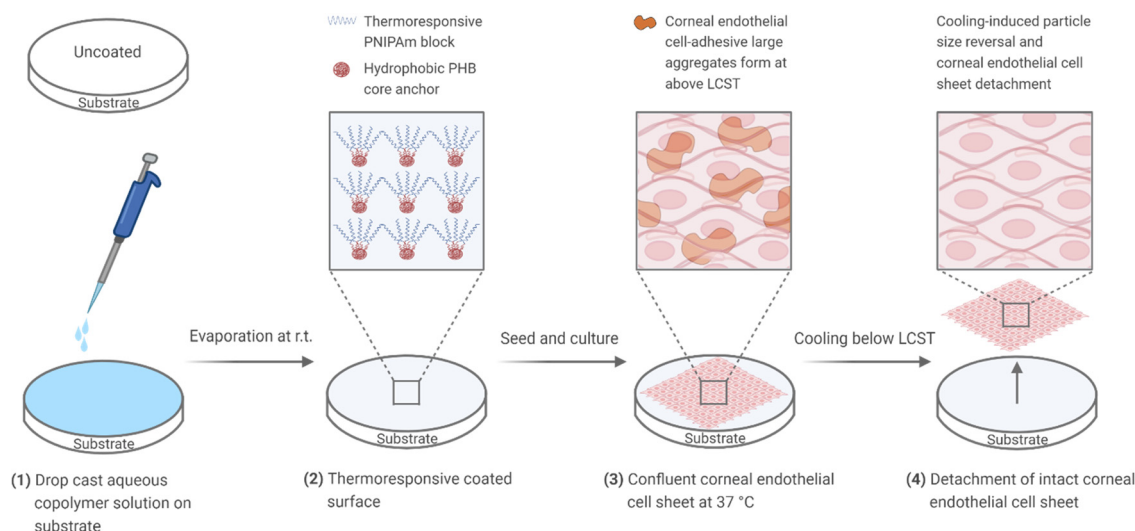

Fig. 1 Conceptual illustration of the thermoresponsive surface coating system. (1) Aqueous copolymer solution is drop-cast onto a substrate. (2) Evaporation of the aqueous solution at room temperature leads to the formation of a uniformly coated thermoresponsive surface. Hydrophobic PHB core acts as an anchor to secure copolymer to the substrate surface *via* hydrophobic interactions. (3) Bovine corneal endothelial cells (BCECs) are seeded onto the substrate and cultured to confluence at 37 °C. The thermoresponsive surface forms large aggregates conducive to cell attachment upon heating to 37 °C (above LCST). (4) Upon cooling below the LCST, the large aggregates reversibly transit to their hydrated state (particle size reversal), dislodging cell adhesion points and causing detachment of an intact cell sheet.

large aggregates that form above LCST. We hypothesize that the incorporation of a biocompatible PHB component can support corneal endothelial cell proliferation and at the same time, the temperature-responsive surface prepared by the triblock copolymer coating can achieve enzyme-free detachment of functional corneal endothelial cell sheets by cooling below its LCST.

2. Experimental section

2.1. Materials

Natural source poly[(R)-3-hydroxybutyric acid] (PHB, Sigma-Aldrich) was purified by dissolving in chloroform at 60 °C followed by filtration through Celite, precipitation in n-hexane, and dried at 60 °C under vacuum for 24 h before use. The M_n and M_w of the purified PHB are 87 kDa and 230 kDa, respectively. N-Isopropylacrylamide (NIPAAm, TCI, >98%) was recrystallized twice from a mixture of toluene and n-hexane (1/3 v/v) and dried at 40 °C under vacuum for 24 h before use. Copper(I) bromide (CuBr, Sigma-Alrich, 99%) was purified by stirring in glacial acetic acid overnight followed by filtration, washing with methanol and diethyl ether successively, and dried at 40 °C under vacuum for 24 h before use. p-Toluenesulfonic acid (PTSA, 98.5%), ethylene glycol (anhydrous, 99%), 2-bromoisobutyryl bromide (98%), 1,1,4,7,10,10-hexamethyltriethylenetetramine (HMTETA, 99%), triethylamine (>99.5%), and 1,4-dioxane (anhydrous, >99%) were obtained from Sigma-Aldrich and used as received. Poly(N-isopropylacrylamide) homopolymer of $M_n \sim$ 40 kDa was bought from Polysciences and used as a control for the cell experiments. Dry nitrogen was used in all reactions.

2.2. Preparation of PHB-diol prepolymer by acid-catalyzed transesterification

The PHB-diol prepolymer was prepared as reported elsewhere.[40,41] In a 500 mL 3-necked round bottom flask, purified PHB (10 g) was dissolved in 100 mL of chloroform at 60 °C under N_2 atmosphere. Upon complete dissolution of PHB, PTSA (4.8 g) and ethylene glycol (18.1 mL) were added successively. The reaction mixture was then allowed to stir at 60 °C under N_2 atmosphere. The progress of the reaction was monitored using GPC (THF as the eluent) until the desired molecular weight was attained. The resultant reaction mixture was then cooled to room temperature and extracted several times with distilled water to remove unreacted ethylene glycol and PTSA. The organic layer was dried using anhydrous $MgSO_4$, filtered, and precipitated into methanol to retrieve the purified polymer. Finally, the purified PHB-diol was dried at 70 °C under vacuum. Yield: 75.6%.

2.3. Synthesis of ATRP macroinitiator (Br-PHB-Br) by bromoesterification

PHB-diol (5.5 g, 2.55 mmol) was dissolved in 34 mL of anhydrous dichloromethane containing 40.7 mmol triethylamine in a 100 mL round-bottomed flask under N_2 atmosphere. The reaction flask was maintained at 4 °C using an ice/water bath. When the PHB-diol had completely dissolved, 20.4 mmol 2-bromoisobutyl bromide dissolved in 4 mL of anhydrous dichloromethane was

added to the flask dropwise through an equalizing funnel. After addition, the temperature was maintained at 4 °C for 2 h and then room temperature for 46 h. The resulting reaction mixture was filtered to remove insoluble triethylamine hydrobromide, concentrated and precipitated in diethyl ether. The crude product was then dissolved in dichloromethane and washed successively with 5 wt% Na_2CO_3 solution and distilled water. The organic phase was dried over anhydrous Na_2SO_4, filtered, concentrated and the product was precipitated in methanol as a white solid. The purified macroinitiator was then dried at room temperature under vacuum. Yield: 57.1%.

2.4. Synthesis of PNIPAm-PHB-PNIPAm triblock copolymers by atom transfer radical polymerization (ATRP)

A molar feed ratio [NIPAm (4.12 g)]/[Br-PHB-Br (0.15 g, M_n = 2470 g mol^{-1} by ^{1}H NMR)]/[CuBr (34.8 mg)]/[HMTETA (116 mg)] of 600 : 1 : 4 : 8 was used. The reaction was performed in a 25 mL Schlenk tube equipped with a magnetic stirrer. NIPAm, Br-PHB-Br, and HMTETA were introduced to the flask containing 4.5 mL of dioxane. After the reactants had completely dissolved, the reaction mixture was thoroughly degassed by three freeze-pump-thaw cycles. The reaction mixture was then frozen in liquid nitrogen and CuBr was quickly added under a nitrogen atmosphere. The Schlenk tube was then subjected to three vacuum-nitrogen refill cycles and thawed, before placing in an oil-bath tempered at 50 °C to initiate polymerization. After 24 h, the reaction was quenched by diluting with THF and exposed to air for 1 h. The catalyst complex was removed by passing the dilute polymer solution through a short neutral aluminium oxide column. A colourless solution was obtained. After the removal of THF under reduced pressure, the crude copolymer was redissolved in a minimum amount of THF and precipitated in excess diethyl ether several times to remove the unreacted NIPAm monomer. The copolymer was then dried under vacuum. The yield after purification was 54% with a NIPAAm conversion of 31.7%.

2.5. Molecular Characterizations

^{1}H NMR (600 MHz) spectra were recorded on a Varian NMR spectrometer at room temperature. Chemical shifts were referenced to the solvent peak (δ = 7.26 ppm for CDCl$_3$). Gel permeation chromatography (GPC) measurements were carried out using Shimadzu SCL-10A and LC-20AD system equipped with two Phenogel 5 μm, 100 and 10^4 Å columns (size: 300 × 4.6 mm) in series and a Shimadzu RID-10A refractive index detector. Tetrahydrofuran (THF) was used as an eluent at a flow rate of 0.30 mL min^{-1} at 40 °C. Monodispersed poly(ethylene glycol) standards were used to obtain a calibration curve. Attenuated total reflectance–Fourier transform infrared (ATR-FTIR) spectra of the polymers were measured using a Bruker FT-IR spectrophotometer; 64 scans were signal-averaged with a resolution of 2 cm^{-1} at room temperature.

2.6. Dynamic light scattering (DLS) measurements

Measurements of micelle size were performed on micelle solutions (0.5 mg mL^{-1}) using a Zetasizer Nano ZS (Malvern Instruments,

This journal is © The Royal Society of Chemistry 2022

J. Mater. Chem. B, 2022, 10, 8407–8418 | 8409

Southborough, MA) with a laser light wavelength of 633 nm at a 173° scattering angle. The micelle size measurement was performed at 25 and 37 °C. The Z-average hydrodynamic diameters of the particles were provided by the instrument. Five independent samples are measured and averaged.

2.7. Critical micelle concentration (CMC) determination

Steady-state fluorescence spectra were recorded on Agilent Cary Eclipse Fluorescence Spectrophotometer. Excitation spectra were monitored at λ_{em} = 390 nm. Slit widths for both excitation and emission sides were maintained at 3.0 nm. Sample solutions of concentrations 0.001–0.1 mg mL^{-1} were prepared by dissolving a predetermined amount of block copolymer in an aqueous pyrene solution of known concentration, and the solutions were equilibrated at room temperature overnight. The concentration of pyrene was fixed at 6.0×10^{-7} M.

2.8. Thermal degradation analysis

Thermogravimetric analyses (TGA) were conducted on TA Instruments TGA Q500. Samples were heated at 20 °C min^{-1} from room temperature to 800 °C under a dynamic nitrogen atmosphere (flow rate = 60 mL min^{-1}).

2.9. Lower critical solution temperature determination

Cloud points were measured using UV-vis spectrophotometer (UV-2600, Shimadzu). Aqueous copolymer solutions (2 mg mL^{-1}) were heated from 25–40 °C at 1 °C increment. Each temperature point was equilibrated for 15 min before recording the transmittance at 450 nm (1 cm path length).

2.10. Coating of Substrates

Aqueous copolymer solutions of different concentrations were prepared by dissolving the copolymers in deionized water (0.001 mg to 1 mg mL^{-1}). Coverglasses were washed successively with distilled water and ethanol, and dried. Silanization of the cleaned coverglasses was then carried out by immersing in 5% methyl trimethoxy silane (MTMS) in toluene for 1 h. After 1 h, the coverglasses were rinsed thoroughly with toluene and ethanol, and allowed to dry completely in a vacuum desiccator overnight. The silanized coverglasses (13 mm diameter) were used as the bare substrate. 100 μL of the aqueous copolymer solutions was drop casted onto the bare substrates and left to dry overnight.

2.11. Contact angle measurements

The contact angles were measured using the sessile drop method. For measurements at 37 °C, the substrates were equilibrated at 37 °C for 20 min on a flat heating plate. 5 μL of pre-heated distilled water (37 °C) was then dropped onto the substrates using a 10 μL micropipette. Image of the water droplet was captured using SONY IMX290 HDMI microscope camera upon equilibrium and analysed using ImageJ (Contact angle plugin). Contact angles were measured at four different parts of the substrates. This process was repeated with two more independent samples and readings were then averaged.

2.12. Cells and media

Bovine corneal endothelial cells (BCECs) were obtained from American Type Culture Collection (ATCC) and cultured as per supplier's instructions. Dulbecco's Modified Eagle's Medium (HyClone) supplemented with 10% fetal bovine serum (Gibco) and 1% penicillin-streptomycin (Gibco) was used as the cell culture medium. BCECs were cultured on tissue culture flasks in an incubator maintained at 37 °C and 5% CO$_2$ until confluence. Upon reaching confluence, the BCECs were passaged using 0.5% trypsin (Gibco), counted using haemocytometer and seeded onto respective culture substrates for subsequent experiments. BCECs at passage +4 from the shipment were used for the experiments. Unless stated otherwise, coverglasses were secured onto 24 well plates using silicone tubes with 0.9 cm inner diameter and subjected to UV sterilisation for 1 h prior to cell seeding.

2.13. *In vitro* cytotoxicity study of copolymers

BCECs were seeded at 5000 cells per well in a 96 well plate and pre-incubated for 24 h in an incubator maintained at 37 °C and 5% CO$_2$. After 24 h, the culture medium was aspirated and 100 μL of polymer solutions of different concentrations dissolved in culture media was dispensed into designated wells. After 48 h of incubation, the culture media was removed. Then, 110 μL of culture media containing 10 μL of CCK-8 cell counting kit solution was added into each well and further incubated for 2 h. The absorbance at 450 nm was then recorded using a microplate reader. Cells cultured in pure culture media were used as the positive control. The absorbance values of the samples were normalized to the positive control and expressed as cell viability (%).

2.14. Cell proliferation assay of BCECs on copolymer coating

The Click-iT™ EdU Proliferation Assay for Microplates was used to study the cell proliferation and cytotoxicity of BCE cells cultured on copolymer coating following the manufacturer's protocol (Click-iT™ EdU Proliferation Assay for Microplates, Thermo), with minor changes to volume used to accommodate the larger wells used in this work. Briefly, BCECs were seeded at 90 000 cells per well and cultured in an incubator maintained at 37 °C and 5% CO$_2$. After three days of culture, the culture media was removed and replaced with 250 μL of culture media containing 50 μL of EdU working solution and further incubated for 4 h. The wells were then fixed, washed, added the reaction mixture, and subsequently stop solution. Fluorescence was then read using a microplate reader (Excitation 568 nm and emission 585 nm).

2.15. Cell sheet detachment by cooling treatment

BCECs were seeded at 90 000 cells per well in 24 well plate and cultured in an incubator maintained at 37 °C and 5% CO$_2$ until a confluent monolayer is formed. Warm media was then aspirated and exchanged with cold 1X PBS solution. The well plates were then maintained at 4 °C in a refrigerator for 20 min. Cell detachment behaviours was observed at 0 min and 20 min upon cooling using a phase contrast microscope.

8410 | *J. Mater. Chem. B*, 2022, **10**, 8407–8418

This journal is © The Royal Society of Chemistry 2022

2.16. Cell viability assay of detached cell sheet

Upon detachment of the cell sheet at 4 °C, the cold 1X PBS was exchanged with warm culture media and placed back into the incubator for 4 h to allow reattachment to the culture substrate. Subsequently, the culture media was removed and 220 μL of culture media containing 20 μL of CCK-8 cell counting kit solution was added and further incubated for 2 h. The absorbance at 450 nm was then recorded using a microplate reader. Confluent BCEC monolayer without the cooling treatment was used as a control.

2.17. Statistical analysis

The statistical analyses of data were conducted using the student's t test or one-way analysis of variance (ANOVA) with Tukey's *post-hoc* test using Origin. All experiments were repeated at least three times and data are presented as mean ± standard deviation.

3. Results and discussion

3.1. Synthesis and characterization of copolymers

The PNIPAAm-PHB-PNIPAAm (NHN) triblock copolymers were synthesized as previously reported by our group with slight modifications (Fig. 2).[42] Low molecular weight PHB-diol (M_n = 2.28 kDa) was first prepared *via* acid-catalyzed transesterification of commercially available high molecular weight PHB (M_n = 87 kDa). The obtained PHB-diol was then reacted with 2-bromoisobutyryl bromide to modify the terminal hydroxyl groups to bromoester groups. The terminal bromide ends then serve as initiator sites for atom transfer radical polymerization (ATRP). The M_n of the resulting PHB-diBr is 2.42 kDa. The increase in molecular weight as determined by GPC (Fig. S1, ESI†) shows that degradation did not occur over the progress of the reaction. The successful substitution of the hydroxyl groups was further verified using ^{1}H NMR spectroscopy (Fig. 3(a) and (b)). The disappearance of the proton signals at 3.8 and 4.2 ppm (ethylene glycol segment of PHB-diol) and the appearance of a new proton signal at ~4.3 ppm shows successful modification of the terminal hydroxyl ends. A sharp proton signal

at ~1.93 ppm belonging to the methyl proton contribution of the 2-bromoisobutyryl group was also observed. The degree of substitution of >92% was determined by comparing the integral ratio of the two proton signals (1.93 and 4.3 ppm).

Finally, the PHB-diBr was used as the macroinitiator for the ATRP of NIPAAm to form the NHN triblock copolymers. Three NHN triblock copolymers of different PNIPAAm block lengths were prepared by adjusting the feed ratio of NIPAAm. ^{1}H NMR spectroscopy was employed to confirm the structures of the samples (Fig. 3(c)). The proton signals at 1.14, 1.4–1.6, 1.78 and 3.95 ppm corresponding to the methyl, methylene, methylidyne protons next to carbonyl group and the methylidyne protons next to the amine belonging to the PNIPAAm segments can be seen clearly. The proton contributions from the PHB central block (methyl proton 1.32, methylene protons 2.49–2.64 and methylidyne protons 5.3 ppm) can also be observed.

Generally, the copolymers are of low dispersity, and the GPC elution profiles (Fig. S1, ESI†) display unimodal peaks indicating that no side products were present in all samples. The increase in molecular weight as determined by both ^{1}H NMR and GPC peak integration proved that the initiator sites were active and chain propagation occurred over the reaction time. Together, the ^{1}H NMR and GPC results demonstrate that the ATRP reactions were well-controlled and the triblock copolymer samples were successfully synthesized. Moreover, the block compositions were determined using ^{1}H NMR integration and TGA (Fig. S2, ESI†). The values agree well with each other, further indicating the successful synthesis. The molecular characteristics of the triblock copolymer samples as well as the starting reactants are summarized in Table 1.

3.2. Micellar formation and thermoresponsive solution properties of copolymers

The critical micelle concentration (CMC) is the minimum amount of copolymer required to form a stable micellar structure in an aqueous environment. To study the micellar formation of the triblock copolymers, the CMC was determined using fluorescence spectroscopy based on pyrene solubilization. Aqueous solutions of
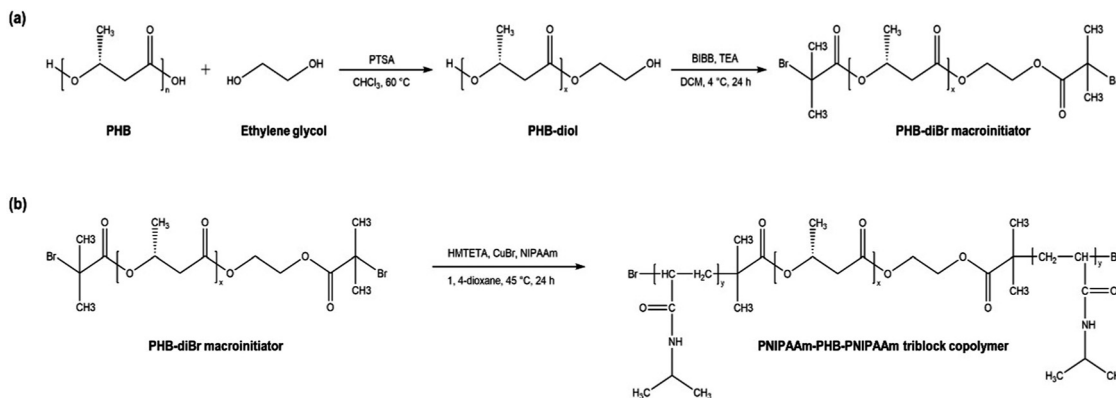

Fig. 2 Synthetic scheme of PNIPAAm–PHB–PNIPAAm (NHN) triblock copolymers. (a) Transesterification of high molecular weight PHB to low molecular weight PHB-diol prepolymer followed by bromoesterification to PHB-diBr macroinitiator. (b) Synthesis of NHN triblock copolymer by Cu(I)-mediated atom transfer radical polymerization.
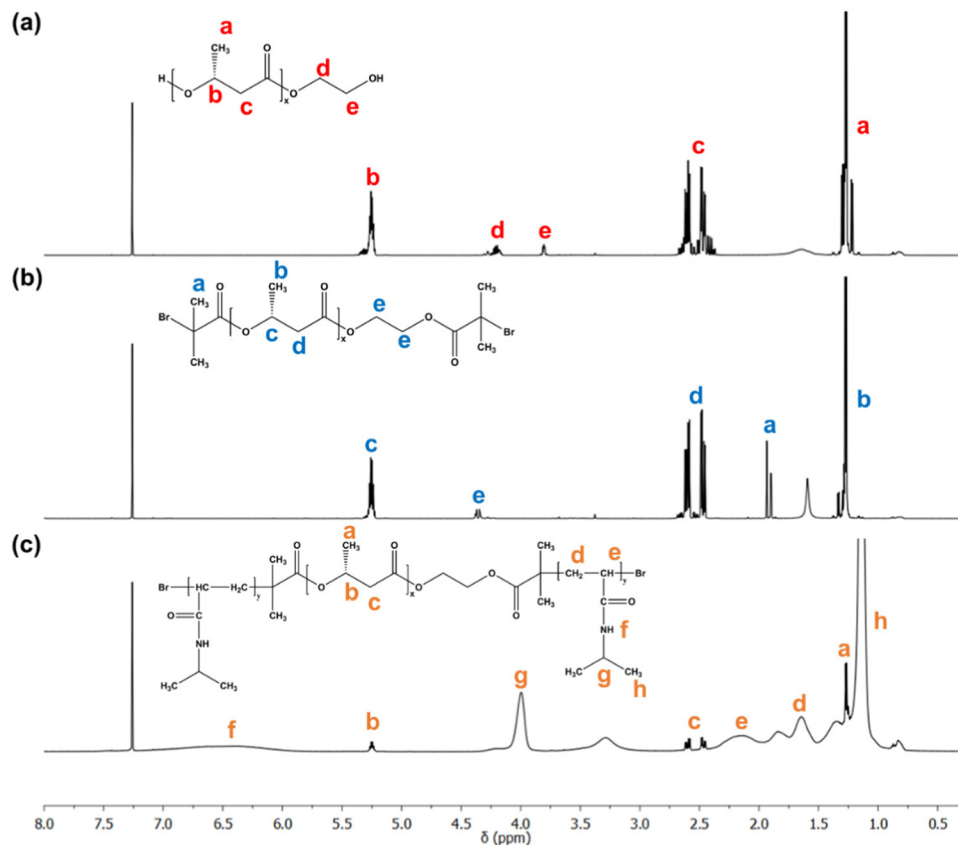
This journal is © The Royal Society of Chemistry 2022

J. Mater. Chem. B, 2022, **10**, 8407–8418 | **8411**

Fig. 3 The 600 MHz ^{1}H NMR spectra of (a) PHB-diol, (b) PHB-diBr, and (c) NHN(65-23-65) in CDCl$_3$ with corresponding peak assignments.

pyrene with a fixed concentration were mixed with varying amount of copolymers. As the concentration of copolymer increases, there is a relocation of pyrene from the aqueous solution to the non-polar PHB core of the copolymer micelle. This pyrene relocation translates to changes in the fluorescence excitation spectra. Specifically, there will be a shift in energy in the wavelength range 333–338 nm. This can be quantified by the intensity ratio of the first and third peaks of the pyrene fluorescence excitation spectra.

To visualise the onset of CMC, the intensity ratio (I_{338}/I_{333}) was plotted against the logarithm function of sample concentration. The CMC is calculated by the intersection point between the best fit line in the range of lower and higher concentrations. As seen in the plots (Fig. 4), upon reaching the CMC, there was a steep increase in intensity ratio as concentration increases.

In contrast, there were only minute changes in the lower concentration range. Generally, the CMC values increased from 13.6 to 14.8 mg L^{-1} as the length of the PNIPAAm blocks in the triblock copolymers increased from 40 to 200. This is due to the enhanced hydrophilicity by the PNIPAAm blocks which destabilizes or interferes with the formation of micelles at low copolymer concentrations.

The thermosensitive property of the triblock copolymers is conferred by the PNIPAAm blocks. In an aqueous environment, PNIPAAm chains exhibit a phenomenon known as the LCST. Below the LCST, the PNIPAAm chains exist in a coil state and is soluble in water. Above the LCST, however, the PNIPAAm chains experience a phase transition from coil-to-globule state and start to precipitate out of the aqueous solution. The coil-to-globule transition can be explained by the change in solvent–solute

Table 1 Molecular characteristics of PNIPAAm-PHB-PNIPAAm triblock copolymers and starting reactants

Sample	$M_n{}^a$ (× 10^3)	$Đ^a$ (M_w/M_n)	$M_n{}^b$ (×10^3)	Copolymer composition^b (wt%)		Copolymer composition^c (wt%)	
				PHB	NIPAAm	PHB	NIPAAm
PHB-diol	2.28	1.18	2.16	—	—	—	—
PHB-diBr	2.42	1.15	2.47	—	—	—	—
NHN(20-23-20)	15.8	1.28	11.5	29.7	70.3	22.4	77.6
NHN(65-23-65)	22.0	1.45	16.0	11.7	88.3	11.8	88.2
NHN(100-23-100)	26.7	1.41	25.0	9.0	91.0	8.9	91.1

^{a} Determined by GPC using THF as eluent. ^{b} Calculated from ^{1}H NMR results. ^{c} Calculated from TGA results.
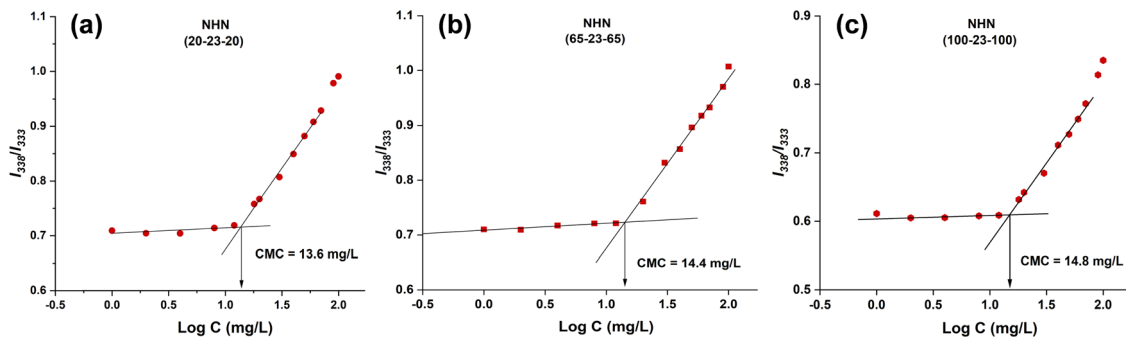
Fig. 4 Plots of the I_{338}/I_{333} ratio of pyrene excitation spectra in water as a logarithmic function of concentration for (a) NHN(20-23-20), (b) NHN(65-23-65), and (c) NHN(100-23-100).

interactions as hydrogen bonds responsible for solvating the PNIPAAm chains become weaker at temperatures above the LCST, resulting in gradual expulsion of water molecules.[43]

In the case of a core–corona triblock copolymer micelle configuration as verified using ^{1}H NMR (Fig. S3, ESI†), the PNIPAAm chains of the corona associate more strongly to the hydrophobic PHB core above the LCST. The implication of this behaviour is that as temperature further increases, intra- and interpolymeric interaction will strengthen, favouring the formation of aggregates. To observe and determine the LCST value of the triblock copolymers, aqueous solutions of the triblock copolymers (2 mg mL^{-1}) were prepared. The copolymer solutions were subjected to temperature increments of 1 °C at regular intervals and the optical absorbance at 450 nm was recorded using UV-vis spectrophotometer (Fig. 5). In this work, the LCST was the temperature at which a 50% reduction in transmittance at 450 nm was observed. The recorded values are shown in Table 2.

The incorporation of hydrophobic segments is known to lower the LCST of PNIPAAm copolymers as demonstrated by numerous studies.[44] The recorded LCST values for this work were 35.1, 34.2 and 32.6 °C, in order of increasing PNIPAAm block length in the copolymers (Table 2). In a well-cited work that first studied the influence of increasing PNIPAAm block

length on LCST values for homopolymer synthesized by ATRP, the reported values with similar molecular weight and LCST determination to this work were 38.9, 34.6 and 33.3 °C.[45] Evidently, the LCST values of the triblock copolymers were lower than the reported values. This is in good agreement with previous observations that incorporation of hydrophobic segments lower LCST values.

To further study the thermosensitive behaviour of the triblock copolymer micelles, the particle size of the micelles was measured at 25 and 37 °C using dynamic light scattering (DLS). The results as illustrated in Fig. 6 using NHN(100-23-100) as the representative sample, showed that the micelles increased in size as the temperature was raised from 25 to 37 °C. This observation is also consistent with the earlier discussion that the formation of aggregation is favoured at temperatures above the LCST, leading to larger particle sizes. The solution properties are summarized in Table 2.

3.3. Preparation of coated substrate and characterizations

In the previous study, a hydrophobic Thermanox coverslip was used as the bare substrate.[38] The hydrophobic PHB component helped to anchor the copolymer to the coverslip through hydrophobic interactions. However, using a plastic substrate like Thermanox makes it challenging to perform subsequent immunofluorescence experiments due to autofluorescence issues. Hence in this work, a coverglass was employed instead. Unmodified commercially available coverglass is hydrophilic due to the presence of hydroxyl groups and is not conducive for this study, which aims to exploit the hydrophobic interactions between the copolymer coating and the bare substrate.
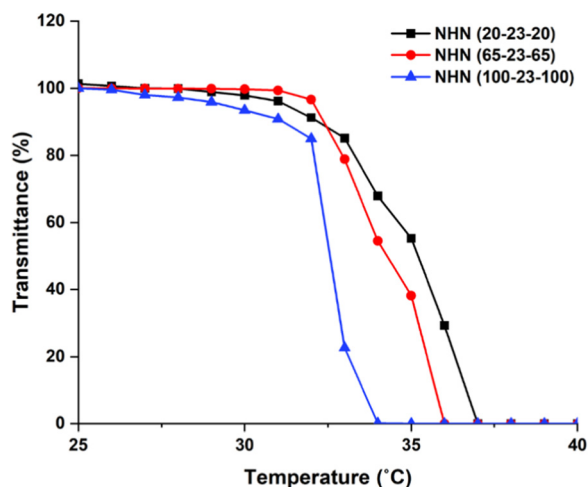

Fig. 5 LCST transitions of the triblock copolymers (2 mg mL^{-1}) measured at 450 nm using UV-vis spectrophotometer.

Table 2 Solution properties of copolymers

Sample	LCST^a (°C)	CMC^b (mg L^{-1})	d^c, 25 °C (nm)	d^c, 37 °C (nm)
NHN(20-23-20)	35.1	13.6	104 ± 4 (0.38)	178 ± 8 (0.27)
NHN(65-23-65)	34.2	14.4	83.4 ± 9 (0.53)	261 ± 12 (0.22)
NHN(100-23-100)	32.6	14.8	42.1 ± 1 (0.39)	485 ± 110 (0.20)

^{a} Determined from UV-vis turbidimetry measurements. ^{b} Determined by pyrene solubilization method. ^{c} Mean Z-average diameters by dynamic light scattering from five individual measurements. Numbers in brackets represent the average polydispersity of the particle size.
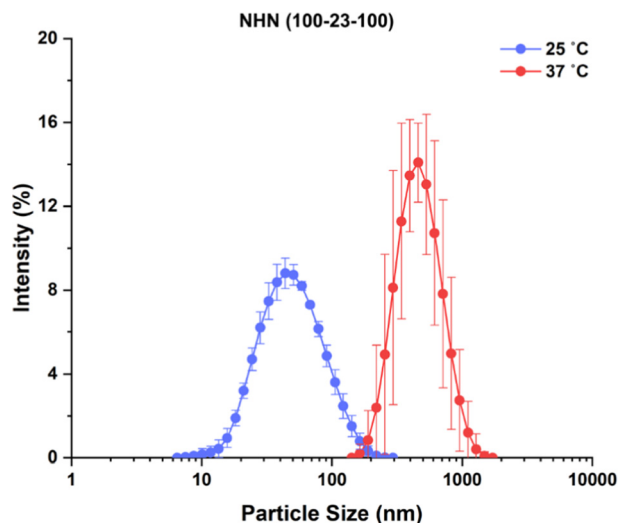
Fig. 6 Particle size distribution profile of NHN(100-23-100) prepared at a concentration of 0.5 mg mL^{-1} in distilled water at 25 °C (blue) and 37 °C (red). Each value represents mean ± SD (n = 5).

increase in contact angle post-silanization, indicating successful modification of the hydrophilic surface to hydrophobic surface. Hence, the silanized coverglass was used for subsequent experiments. Upon drop-casting the copolymer solutions on the hydrophobic coverglass, a similar observation (to the previous work)[38] that a more uniform coverage was noted for the copolymers as compared to the homopolymer control (data not shown).

Next, the selection of the copolymer coating with the highest thermal response is imperative to provide sufficient force for successful detachment of a cell sheet. The "thermal response" is defined in this section as the difference in the contact angle when the substrate is heated to 37 °C from room temperature. The change in contact angle of the substrates coated by three different copolymers of increasing PNIPAAm lengths was compared at two temperatures, 20 and 37 °C (Fig. 7(b)). As expected, the triblock copolymer, NHN(100-23-100) with the longest PNIPAAm chains displayed the highest thermal response and this was in accordance with the steeper drop in optical transmittance (at 450 nm) as determined by the LCST turbidity measurements.

Therefore, silanization of the coverglass was performed to introduce methyl groups onto the surface, thereby rendering it hydrophobic.[46] As seen from Fig. 7(a), there was a significant

Subsequently, the effect of coating density on thermal responses was compared using NHN(100-23-100) triblock copolymer and a commercially bought homopolymer PNIPAAm ($M_{\mathrm{n}} \sim$ 40 kDa) (Fig. 7(c) and (d)). In general, NHN(100-23-100)
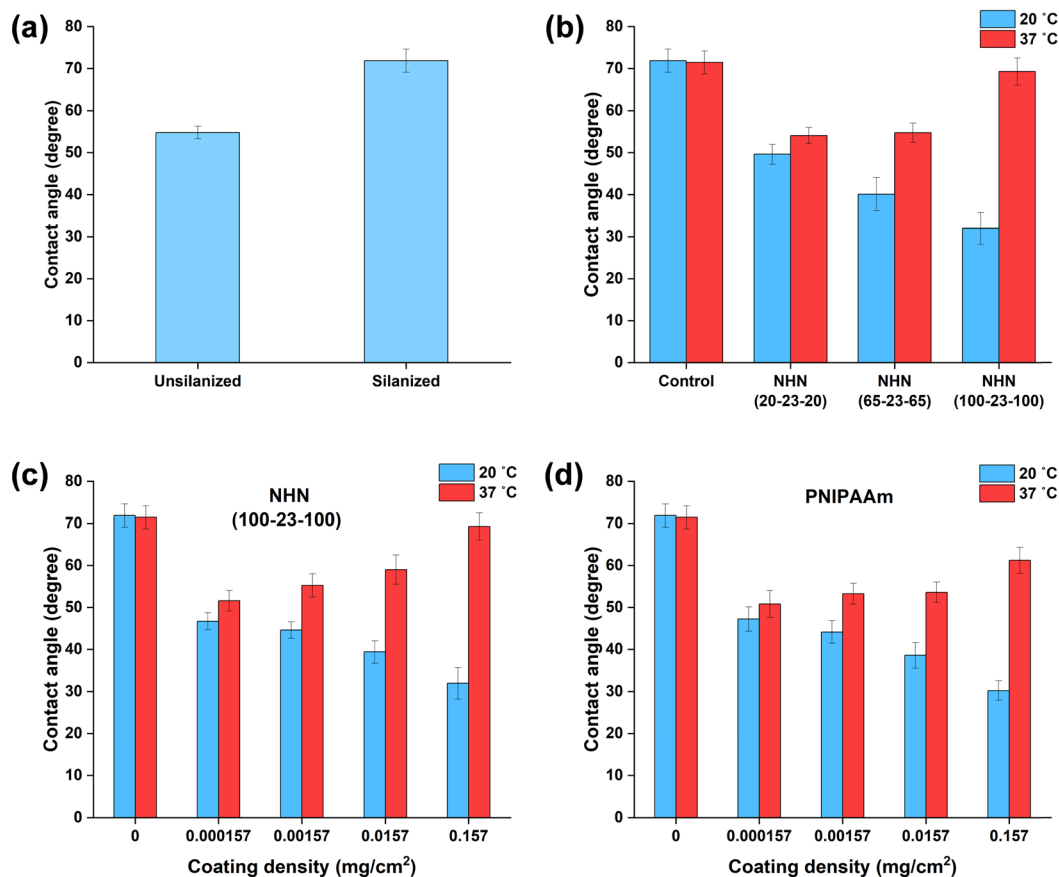

Fig. 7 Contact angle measurements of (a) unsilanized and silanized coverglasses at 20 °C, (b) comparison of thermal responses between the different triblock copolymers at 0.157 mg cm^{-2} coating density, (c) effect of coating density on the thermal response for NHN(100-23-100) coated coverglass, and (d) effect of coating density on the thermal response for PNIPAAm homopolymer coated coverglass. Each value represents the mean ± SD (n = 12).

8414 | J. Mater. Chem. B, 2022, 10, 8407–8418

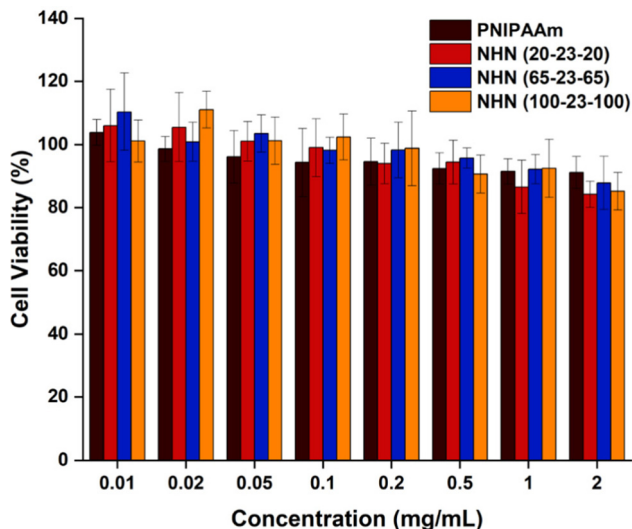This journal is © The Royal Society of Chemistry 2022

Fig. 8 Cell viability of BCE cells incubated with varying concentrations of PNIPAAm homopolymer and NHN copolymer samples as determined using the CCK-8 assay. Each value represents the mean ± SD (n = 6).

exhibited slightly higher thermal responses for the four coating densities tested. This could be attributed to the less uniform coating of the PNIPAAm homopolymer upon drop casting and drying.

3.4. *In vitro* cytotoxicity study of the triblock copolymers

Cytotoxicity of the PNIPAAm control homopolymer as well as all the triblock copolymers was assessed using CCK-8 cell viability assay (Fig. 8). BCECs were cultured in culture media containing various polymer concentrations. Overall, the polymers did not exhibit significant toxicity even at a high concentration of 2 mg mL^{-1}. Different lengths of PNIPAAm also did not seem to present any differences in cytotoxicity. Together, this experiment demonstrated that the control homopolymer and synthesized copolymers were non-cytotoxic in this application as the amount used for subsequent experiments were considerably lesser than 2 mg mL^{-1}.

3.6. EdU proliferation assay of BCECs on coated substrates

The variation of coating densities may affect the surface chemistry and energy such as the water contact angle changes as shown in Fig. 7(c) and (d). It has been demonstrated that variation of water contact angles may affect cellular attachment to biomaterials and subsequently, proliferation.[47] Thus, by varying the coating densities used in this work should affect the proliferation rate of the BCECs differently. To determine the optimal coating density for BCEC proliferation, BCECs were seeded at 90 000 cells per well and cultured on substrates of varying coating densities of NHN(100-23-100). After 3 days of culture, culture media was exchanged with culture media containing EdU and further incubated for 4 h before the EdU proliferation assay was performed to quantify the proliferation rates using a microplate reader.

EdU is incorporated into the DNA of actively dividing cells, providing a sensitive method to assay proliferation rates.[48] The assay revealed that there was an optimal coating density (0.0157 mg cm^{-2}) among the four coating densities screened that resulted in the highest relative fluorescence intensity of 114 ± 7% (Fig. 9(a)). On the other hand, the coating density of 0.157 mg cm^{-2} resulted in the lowest value of 97 ± 3%. The differences in the proliferation rates were statistically significant hence verifying that the variation in coating densities will influence the proliferation rate of the BCECs differently.

Next, the effect of the polymer coating used (at the same coating density) on the proliferation rate of BCECs was evaluated (Fig. 9(b)). It was found that at the same coating density, BCECs cultured on the PNIPAAm-coated substrate exhibited lower proliferation rate (85 ± 8%) that was significantly lower than the BCECs cultured on the NHN(100-23-100)-coated substrate (114 ± 7%). This may be attributed to a few factors such as the less uniform coating, the macromolecular architecture (*i.e.*, homopolymer *vs.* triblock copolymer) and the slight differences in contact angles at 37 °C. All of which may affect how the BCECs adhere and respond to the culture substrate. Since a high proliferation rate was required in this application, NHN(100-23-100) with the
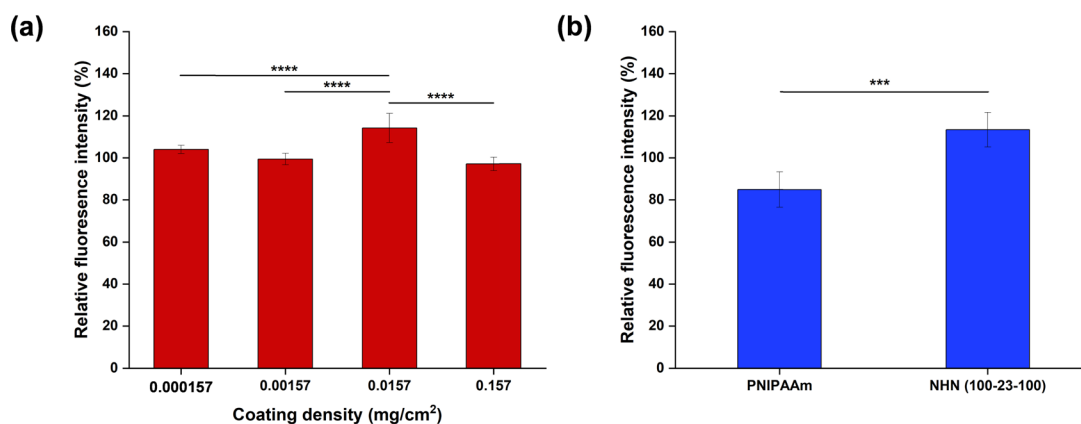

Fig. 9 Relative fluorescence intensity of EdU proliferation assay for bovine corneal endothelial cells cultured on (a) NHN(100-23-100)-coated substrates with varying coating densities and (b) PNIPAAm- and NHN(100-23-100)-coated substrates. The fluorescence intensity was relative to uncoated substrate control. Each value represents the mean ± SD (n = 12). The statistical significance was computed using one-way ANOVA for (a) and student's t test for (b). (***p < 0.001, ****p < 0.0001).
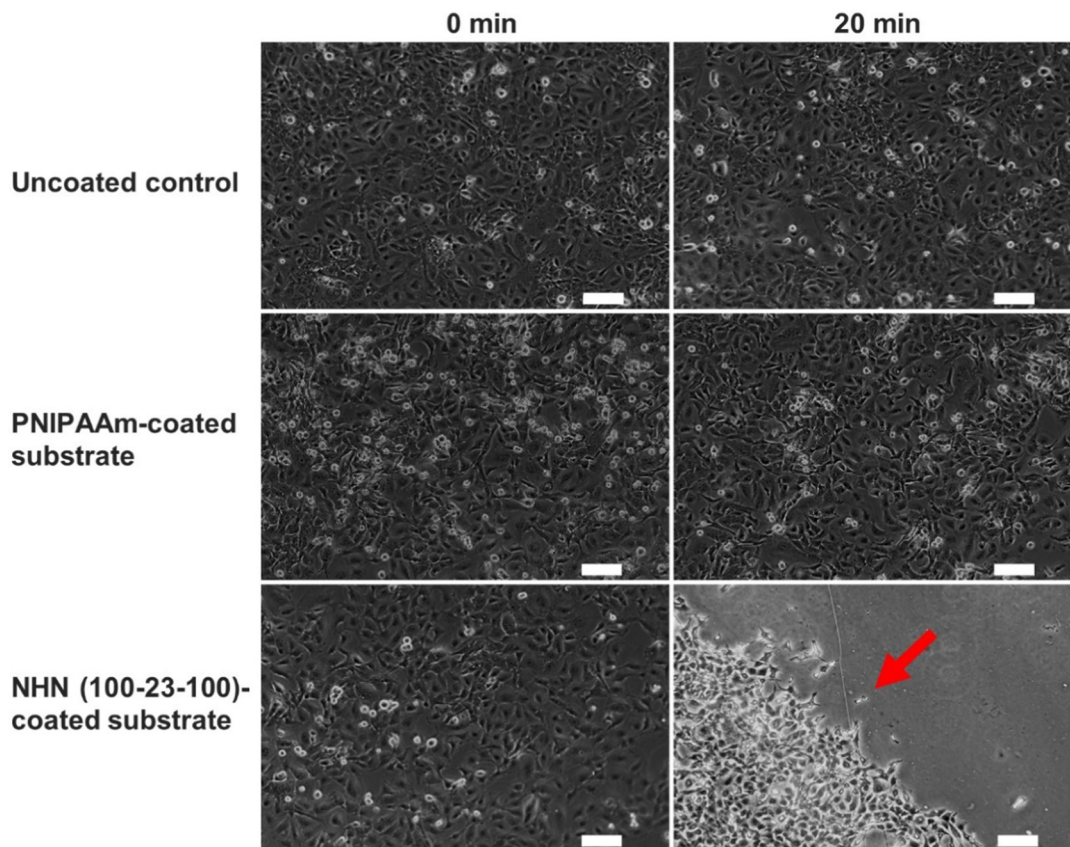
Fig. 10 Phase contrast images of cultured bovine endothelial cells at 0 min and 20 min after cooling at 4 °C for uncoated substrate, PNIPAAm-coated substrate, and NHN(100-23-100)-coated substrate (Scale bar = 100 µm). Coating density used for both PNIPAAm and NHN(100-23-100) coatings = 0.0157 mg cm^{-2}. *Red arrow indicates the direction of cell sheet detaching.

optimal coating density of 0.0157 mg cm^{-2} was used for subsequent experiments.

3.7. Cell sheet detachment by cooling treatment and viability assay

Finally, the cell sheet detachment capability of the coated substrates was studied. BCECs were seeded at a density of 90 000 cells per well. After three days of culture, the culture media was exchanged with cold 1X PBS and cooled at 4 °C for 20 min. As observed in Fig. 10, no noticeable changes to the cell monolayer were observed for the uncoated control and the PNIPAAm-coated substrate. However, for the NHN(100-23-100)-coated substrate, there was a clear detachment of the cell monolayer with the red arrow indicating the direction of detachment. This suggested that the phase transition of the triblock copolymer at a coating density of 0.0157 mg cm^{-2}, provided sufficient changes in surface energy that enabled the detachment of the cell monolayer as an intact sheet. The failure of the PNIPAAm coating to detach the cell monolayer may be due to the lack of a hydrophobic anchor to the coverglass. Hence, instead of acting as a stable substrate for cell culture, the PNIPAAm homopolymer may be freely suspended in the culture media. Therefore, even with a thermal-induced phase transition of the homopolymer, insufficient surface energy

changes may contribute to its inability to detach the cell monolayer.

Cooling treatment may adversely affect the viability of the detached cell sheet due to reduced metabolic activity and protein synthesis.[49] Thus, it is imperative to conduct a viability assay of the BCE cell sheet after detachment by the cooling
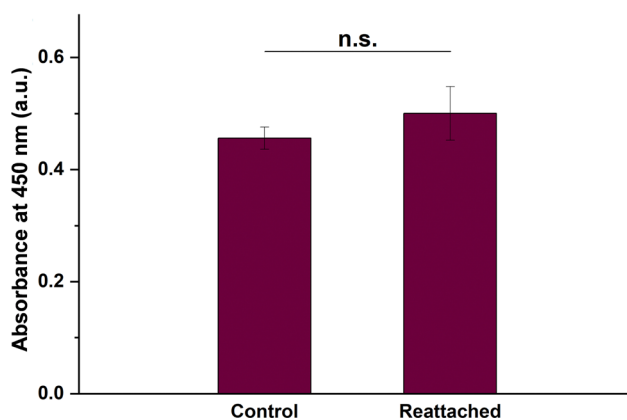

Fig. 11 Cell viability of the BCE cell sheet after detachment by cooling treatment and reattachment as quantified using the CCK-8 assay. BCE cell sheet without the cooling treatment was used as a control. Each value represents the mean ± SD (n = 3). (n.s.: not statistically significant).

8416 | J. Mater. Chem. B, 2022, **10**, 8407–8418

This journal is © The Royal Society of Chemistry 2022

treatment. We allowed the detached cell sheet to re-attach to a coverglass and compared the viability to a BCE cell sheet control without the cooling treatment. We found no significant differences in the viabilities between the two groups (Fig. 11). This provides promising evidence for future *in vivo* transplantation studies.

4. Conclusions

The triblock copolymer PNIPAAm-PHB-PNIPAAm was synthesized and explored as a novel surface coating for the detachment of bovine corneal endothelial cell sheet. By utilizing the facile method of drop casting, the use of costly equipment and material wastage can be avoided. Importantly, the incorporation of a central hydrophobic and biocompatible PHB block enabled the anchoring of the coating to the bare substrate as well as enhance proliferation rate of the BCECs studied. Effective detachment of an intact cell sheet was also demonstrated *via* a cooling treatment, and the viability of the detached cell sheet was found to be unaffected by the cooling. This work may potentially inspire more studies involving the non-covalent thermoresponsive polymer coatings for corneal tissue engineering and other tissue engineering applications.

Conflicts of interest

The authors declare no conflict of interest.

Acknowledgements

References

1 M. R. Aguilar and J. San Román, *Smart polymers and their applications*, Woodhead publishing, 2019.
2 J. Kobayashi, Y. Akiyama, M. Yamato and T. Okano, in *Comprehensive Biotechnology*, ed. M. Moo-Young, Pergamon, Oxford, 3rd edn, 2019, pp.457–470, DOI: 10.1016/B978-0-444-64046-8.00275-5.
3 V. V. Khutoryanskiy and T. K. Georgiou, *Temperature-Responsive Polymers: Chemistry, Properties, and Applications*, Wiley, New York, 2018.
4 M. Liu, Y. T. Wen, X. Song, J. L. Zhu and J. Li, *Carbohydr. Polym.*, 2019, **219**, 280–289.
5 S. Lanzalaco and E. Armelin, *Gels*, 2017, **3**, 36.
6 N. M. Smeets, E. Bakaic, M. Patenaude and T. Hoare, *Acta Biomater.*, 2014, **10**, 4143–4155.
7 M. N. Mohammed, K. B. Yusoh and J. H. B. H. Shariffuddin, *Mater. Express*, 2018, **8**, 21–34.
8 K. M. Rao, K. S. V. K. Rao and C.-S. Ha, *Gels*, 2016, **2**, 6.
9 L. Klouda, *Eur. J. Pharm. Biopharm.*, 2015, **97**, 338–349.
10 L. Tang, L. Wang, X. Yang, Y. Feng, Y. Li and W. Feng, *Prog. Mater. Sci.*, 2021, **115**, 100702.
11 W. W. M. Soh, R. Y. P. Teoh, J. Zhu, Y. Xun, C. Y. Wee, J. Ding, E. S. Thian and J. Li, *Biomacromolecules*, 2022, **23**, 3477–3492.
12 M. Liu, J. Zhu, X. Song, Y. Wen and J. Li, *Gels*, 2022, **8**, 441.
13 J. L. Zhu, S. W. K. Yu, P. K. H. Chow, Y. W. Tong and J. Li, *Biomaterials*, 2018, **180**, 163–172.
14 G. Agrawal and R. Agrawal, *Small*, 2018, **14**, 1801724.
15 A. Bordat, T. Boissenot, J. Nicolas and N. Tsapis, *Adv. Drug Delivery Rev.*, 2019, **138**, 167–192.
16 X. Song, Y. Wen, J.-L. Zhu, F. Zhao, Z.-X. Zhang and J. Li, *Biomacromolecules*, 2016, **17**, 3957–3963.
17 X. Song, Z. Zhang, J. Zhu, Y. Wen, F. Zhao, L. Lei, N. Phan-Thien, B. C. Khoo and J. Li, *Biomacromolecules*, 2020, **21**, 1516–1527.
18 X. Song, J.-l Zhu, Y. Wen, F. Zhao, Z.-X. Zhang and J. Li, *J. Colloid Interface Sci.*, 2017, **490**, 372–379.
19 V. Kozlovskaya and E. Kharlampieva, *ACS Appl. Polym. Mater.*, 2019, **2**, 26–39.
20 K. Nagase, M. Yamato, H. Kanazawa and T. Okano, *Biomaterials*, 2018, **153**, 27–48.
21 Y. Wen, N. N. Mensah, X. Song, J. Zhu, W. S. Tan, X. Chen and J. Li, *Chem. Commun.*, 2022, **58**, 681–684.
22 K. Okabe, N. Inada, C. Gota, Y. Harada, T. Funatsu and S. Uchiyama, *Nat. Commun.*, 2012, **3**, 1–9.
23 E. Ho, A. Lowman and M. Marcolongo, *Biomacromolecules*, 2006, **7**, 3223–3228.
24 E. A. Ksendzov, P. A. Nikishau, I. M. Zurina, V. S. Presniakova, P. Timashev, Y. A. Rochev, S. Kotova and S. V. Kostjuk, *ACS Appl. Polym. Mater.*, 2022, **4**, 1344–1357.
25 J. Akimoto and Y. Ito, in *Sustainability & Green Polymer Chemistry Volume 1: Green Products and Processes*, ACS Publications, 2020, pp.159–172.
26 M. Li, J. Ma, Y. Gao and L. Yang, *Cytotherapy*, 2019, **21**, 3–16.
27 H. Takahashi and T. Okano, *Adv. Drug Delivery Rev.*, 2019, **138**, 276–292.
28 Y. Lu, W. Zhang, J. Wang, G. Yang, S. Yin, T. Tang, C. Yu and X. Jiang, *Int. J. Oral Sci.*, 2019, **11**, 1–13.
29 Z. Jiang, J. He, X. Wang, D. Zhu, N. Li, L. Ren and G. Yang, *Colloids Surf., B*, 2022, 112661.
30 K. Matsuura, R. Utoh, K. Nagase and T. Okano, *J. Controlled Release*, 2014, **190**, 228–239.
31 J. M. Kelm and M. Fussenegger, *Adv. Drug Delivery Rev.*, 2010, **62**, 753–764.
32 H.-L. Huang, H.-W. Hsing, T.-C. Lai, Y.-W. Chen, T.-R. Lee, H.-T. Chan, P.-C. Lyu, C.-L. Wu, Y.-C. Lu and S.-T. Lin, *J. Biomed. Sci.*, 2010, **17**, 1–10.
33 G. O. Waring III, W. M. Bourne, H. F. Edelhauser and K. R. Kenyon, *Ophthalmol.*, 1982, **89**, 531–590.
34 M. M. Jumblatt, D. M. Maurice and J. P. McCulley, *Invest Ophthalmol. Visual Sci.*, 1978, **17**, 1135–1141.
35 N. C. Joyce, *Prog. Retinal Eye Res.*, 2003, **22**, 359–389.

This journal is © The Royal Society of Chemistry 2022

J. Mater. Chem. B, 2022, **10**, 8407–8418 | 8417

36 T. Ide, K. Nishida, M. Yamato, T. Sumide, M. Utsumi, T. Nozaki, A. Kikuchi, T. Okano and Y. Tano, *Biomaterials*, 2006, **27**, 607–614.

37 L. Li, Y. Zhu, B. Li and C. Gao, *Langmuir*, 2008, **24**, 13632–13639.

38 X. J. Loh, W. C. D. Cheong, J. Li and Y. Ito, *Soft Matter*, 2009, **5**, 2937–2946.

39 X. J. Loh, J. Gong, M. Sakuragi, T. Kitajima, M. Liu, J. Li and Y. Ito, *Macromol. Biosci.*, 2009, **9**, 1069–1079.

40 G. R. Saad, Y. Lee and H. Seliger, *J. Appl. Polym. Sci.*, 2002, **83**, 703–718.

41 Z. Špitalský, I. Lacík, E. Lathova, I. Janigova and I. Chodak, *Polym. Degrad. Stab.*, 2006, **91**, 856–861.

42 X. J. Loh, Z.-X. Zhang, Y.-L. Wu, T. S. Lee and J. Li, *Macromolecules*, 2009, **42**, 194–202.

43 K. Kubota, S. Fujishige and I. Ando, *Polym. J.*, 1990, **22**, 15–20.

44 C. Zhao, Z. Ma and X. Zhu, *Prog. Polym. Sci.*, 2019, **90**, 269–291.

45 Y. Xia, X. Yin, N. A. D. Burke and H. D. H. Stöver, *Macromolecules*, 2005, **38**, 5937–5943.

46 Z. Hórvölgyi, M. Máté, A. Dániel and J. Szalma, *Colloids Surf., A*, 1999, **156**, 501–507.

47 K. L. Menzies and L. Jones, *Optom. Vis. Sci.*, 2010, **87**, 387–399.

48 E. Kotogány, D. Dudits, G. V. Horváth and F. Ayaydin, *Plant Methods*, 2010, **6**, 5.

49 A. Roobol, M. J. Carden, R. J. Newsam and C. M. Smales, *FEBS J.*, 2009, **276**, 286–302.

8418 | *J. Mater. Chem. B*, 2022, **10**, 8407–8418

This journal is © The Royal Society of Chemistry 2022